American Mineralogist
Vol. 57, pp. 1664–1680 (1972)

MICROSTRUCTURAL INVESTIGATION OF BALLAS DIAMOND

LUCIEN F. TRUEB AND CHARLES S. BARRETT,
Metallurgy and Materials Science Division, Denver Research Institute, University of Denver, Denver, Colorado 80210

ABSTRACT

Brazilian ballas consists of dense, globular aggregates of anhedral diamond crystallites with an average diameter of the order of 40 microns. The grain boundaries, which are often outlined by impurities and inclusions, are interlocked in complex sawtooth patterns and fracture is almost exclusively transgranular. Inclusions in the form of dark flakes and small crystals are often found in clusters throughout the stones and consist mainly of garnets, magnetite, biotite, zircon, and quartz. Dislocation motion in the diamond crystallites is significantly inhibited by pinning, presumably due to impurities in the lattice, resulting in kinking and the formation of elongated dislocation loops. The crystallites have a well developed preferred orientation, each radial direction being an axis of a [110] fiber texture. The orientation of the crystallites around each texture axis is random.

INTRODUCTION

Ballas diamonds, found only in Bahia, Brazil, the Premier Mine in South Africa, and the Urals, are the least investigated of the various types of polycrystalline diamond. Brazilian carbonado and Central–African carbon, both of which are varieties of the so–called black diamond, have recently been characterized in detail by Trueb and Butterman (1969) and by Trueb and de Wys (1969, 1971). Carbonado has been synthesized by means of static high pressure both in the United States (Wentorf and Bovenkerk, 1961) and the Soviet Union, and the microstructural features of this material have been published by Malov (1969). Explosively synthesized polycrystalline diamond has also received much attention in recent years (Mears and Bowman, 1966; and Trueb, 1968, 1971). Literature on ballas, however, is very scarce, even though the material is not particularly rare and is considered to be the toughest of all types of diamond. It is often used in shaping tools (Cumming, 1951).

The earliest reference to ballas available to us is by Kunz (1884); it describes the external appearance of some perfectly spherical specimens from Brazil. Sutton (1928) states that it is a good electrical conductor, has a specific gravity that may be higher than that of monocrystalline diamond, and usually consists of translucent spheres

with light to dark-gray color, sometimes pink to brown, with greater cohesion than ordinary bort and without true cleavage. Fractured pieces suggest a radial structure from a central core. Williams (1932) indicates that common inclusions in diamond such as garnet and ilmenite were never found in ballas and that the total non-diamantiferous matter is less than one percent, the ash consisting mainly of silica and oxides of aluminum, iron, calcium, and magnesium.

In all subsequent references on ballas, it is invariably referred to as globular aggregates of radially arranged diamond crystals (Grodzinski, 1943). This ill-defined model, which was not confirmed by Fischer (1961), appears to be based on observations by Sutton (1928).

The synthesis of ballas by static high pressure has been claimed by Kalishnikov and co-workers (1967), but the information given in their paper is extremely vague, indicating only that spherical polycrystalline globules with a complex inner structure were obtained. One of us (LFT) was told by V. I. Bakul during a recent visit at the Institute for Superhard Materials in Kiev, USSR, that the synthetic ballas consists of globules with a diameter of several millimeters; no details concerning the microstructure of the material could be obtained; it was also learned that Soviet investigators consider synthetic ballas to be particularly useful in shaping tools and drawing dies. Nikol'skaya *et al.* (1968) have published a note in which they conclude that the material has a preferred orientation in which the [111] direction is radial. The basis for this conclusion is not obvious; it does not seem to be supported by the X-ray diffraction patterns in the note.

The present investigation was undertaken with the aim of relating the unique physical characteristics of natural ballas, particularly its cutting ability and toughness, to its substructure which had never been adequately investigated by modern physical methods.

Experimental and Discussion

Origin

A total of forty-eight randomly chosen specimens of ballas supplied by two separate dealers were studied in the course of this investigation. They were of standard commercial grade and imported from Brazil. Such stones are known to be gathered by hand in alluvial deposits and pass through at least six sets of dealers before reaching New York. Thus the exact origin of the specimens could not be ascertained, although it is likely that they originated from Bahia province where most ballas is found.

Morphology

The diameter of the specimens varied from 3 to 12.5 mm, most of them being in the 5 to 8 mm range; a few were fully spheroidal, but the majority were only fragments of spheres. In these instances the specimens had the shape of lemon wedges, or pyramids with spheroidal bases and three to four ridges radiating from the center of the fractured interface. All specimens were translucent to various degrees, their color ranging from green–gray and brown–gray to amber, pale–yellow, and pure white. The outer region within the first millimeter was often significantly darker than the inside of the stones. Stained areas were observed occasionally, particularly around the larger inclusions.

Some stones were crushed in a large vise, the specimens being wrapped in several layers of bond paper. Aside from the formation of variable amounts of powder, this resulted in break–up into wedge–shaped fragments with relatively flat fracture interfaces. Examination of the minute fragments in the microscope revealed that many of them were needle shaped; X–ray diffraction showed that the needles were polycrystalline. The fragments adhering to the vise jaws after crushing were discarded to avoid contamination with iron.

Surface Structure

The polycrystalline nature of the specimens was evident from their outer structure, which was characterized by a pattern of more or less polished facets separated by groove-shaped grain boundaries. These features can be observed in Figure 1A. In some instances, crystallites having the shape of octahedra or distorted octahedra could be distinguished; furthermore, individual facets sometimes exhibited a pattern of steps. The relative orientation of such octahedra as well as the direction of the step patterns in adjacent grains (Fig. 1B) suggested preferred orientation of the crystallites.

At high magnifications, the surface showed evidence of polishing, micropitting, abrasion, and localized fracture (Figs. 2A and 2B), presumably resulting from the erosional processes and transport in river–beds. In some specimens, the surface was pockmarked by elongated pits and grooves up to 1 mm deep. Several types of inclusions were observed both on the outer surface and throughout the crystallites; they are described in detail in a subsequent paragraph.

Internal Structure

Because of the relatively high cost of ballas, non–destructive methods were used extensively for investigating its internal structure.

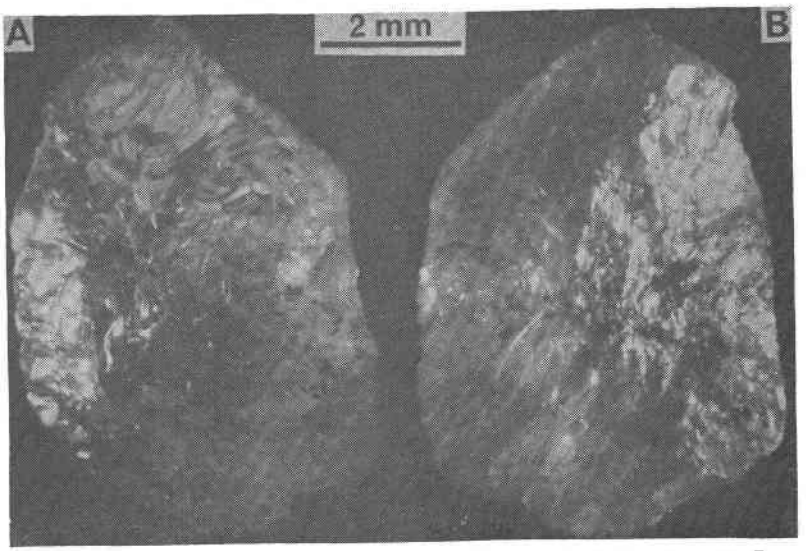

FIG. 1. Photomicrograph of ballas fragment. A: Outer, spherical surface. B: Inner, fractured surface. The black spots are inclusions.

However, a few specimens were fractured and partly crushed as described above for electron microscopy, electron probe microanalysis, and emission spectrograph analysis.

As previously mentioned, the fracture interface of ballas, as viewed with the naked eye and low-power magnification, often assumes the shape of a wedge or pyramid and exhibits lines radiating from an apex situated near the center of the stone. This appearance has usually been attributed to a radial arrangement of crystallites (Kunz, 1884;

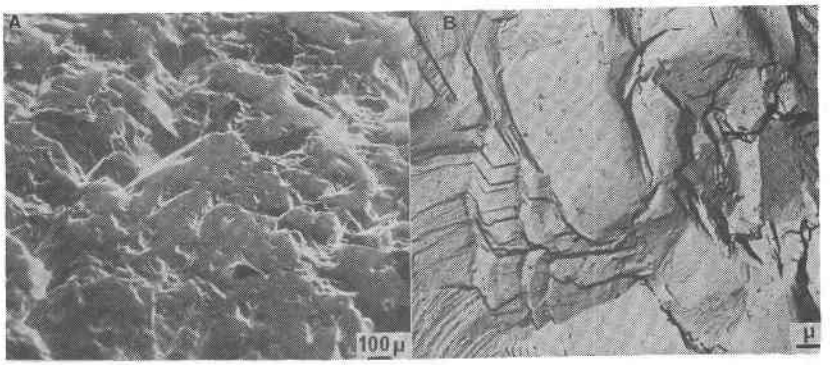

FIG. 2. Hemispherical outer surface of ballas. A: Scanning electron micrograph. B: Electron micrograph of replica.

and Sutton, 1928), and can clearly be seen by light-optical microscopy or scanning electron microscopy, as shown in Figure 3. The fact that many needle-shaped fragments are formed when crushing ballas also suggests that some radial characteristic of the crystallites exists.

Because of the difficulties involved in polishing ballas for optical microscopy, the size of the crystallites was determined by the Berg-Barrett technique (Barrett, 1945). Copper $K\alpha$ radiation was used, and the fractured interfaces of the specimens were placed directly on the photographic plate. The patterns were recorded on fine-grain nuclear emulsion (Ilford L4 and Ilford G plates); they were of the type shown in Figure 4 and consisted of large numbers of individual 111, 220, and 311 reflections. For the 220 and 311 reflections, the diffracted beams were nearly perpendicular to the plate; therefore they are registered in the emulsion with negligible distortion. Since the diffracted rays form images of those grains which are in a reflecting position, the crystallite size was determined after ten or twenty-fold optical magnification of 220 and 311 reflections. It was found that the individual reflections had sizes consistent with crystallites varying from about 10 to over 200 microns, with a sharp maximum

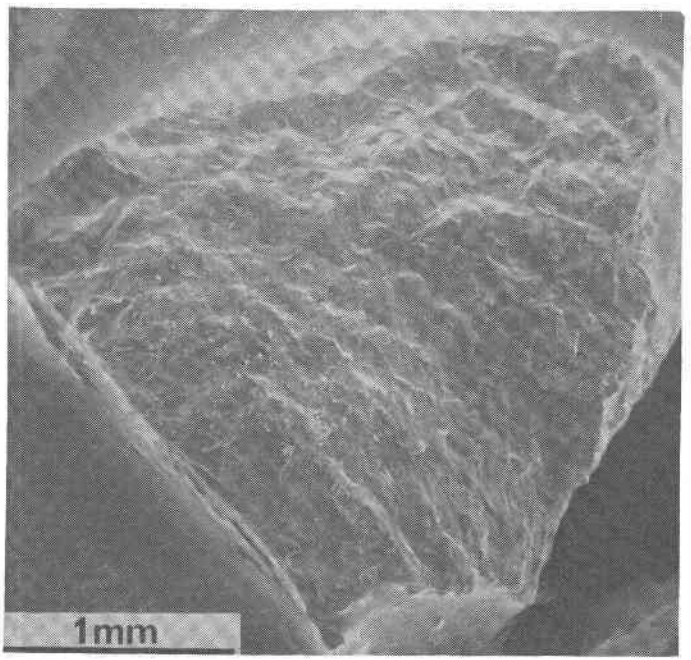

FIG. 3. Fracture surface of ballas fragment (scanning electron micrograph).

in the particle–size distribution near the 30 to 40 micron range. For the nine samples investigated in this manner, the average reflection size ranged from 33 to 41 microns, the overall average being 37 microns, and these sizes can be taken as being close to the crystallite sizes. Measurements from Berg–Barrett patterns tend to emphasize the largest crystallite sizes and thus indicate an upper limit to a true average value; however, the indicated order of magnitude of the crystallite size was confirmed by light and electron microscope observations.

Examination of fracture interfaces of ballas by light–optical and electron microscopy revealed that most of the crystallites were more or less equiaxed in shape and anhedral. Figure 5A shows that the interfaces of individual crystallites are characterized by patterns of fracture steps. Fracture was almost exclusively transgranular, which indicates a high degree of cohesion between crystallites. This effect may be related to the jagged appearance of the grain boundaries, which are tightly interlocked in complex zig–zag patterns as shown in Figure 5B.

For transmission electron microscopy, a dispersion of finely crushed ballas in absolute methanol was left to dry on a carbon–coated specimen grid. The fragments that were electron–transparent at 100 kV were often found to include grain boundaries. Selected area electron

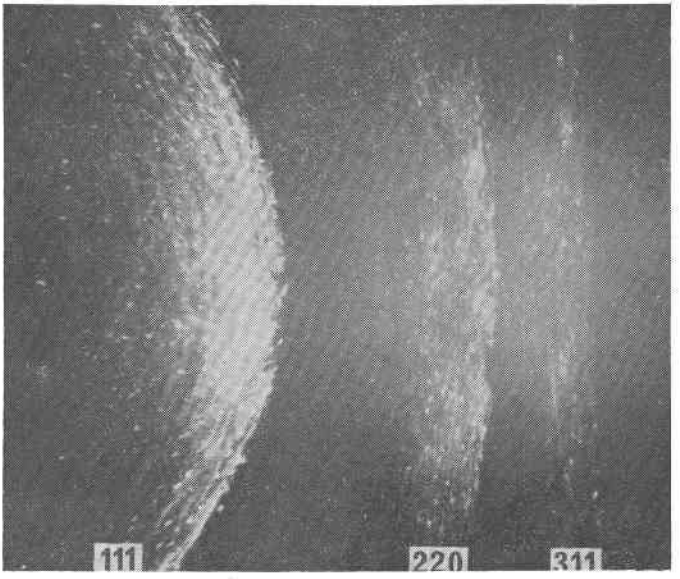

FIG. 4. Berg–Barrett diagram of ballas showing 111, 220, and 311 reflections.

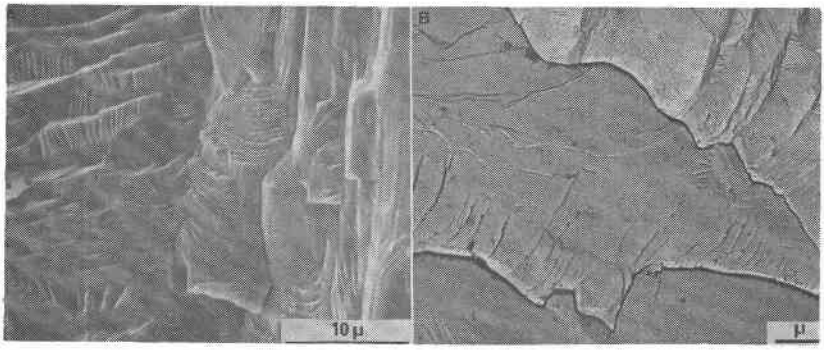

FIG. 5. Fracture interface of ballas. A: Scanning electron micrograph. B: Electron micrograph of replica.

diffraction (SAD) showed that both high– and low–angle boundaries occurred. Figure 6 includes a typical low–angle boundary associated with the set of parallel dislocations on the left side of the picture. The SAD pattern in Figure 6 shows that the pair of 220 reflections are separated by 3.5°. Inside of the crystallites, the density of dislocations was relatively high, with an average value of $3.2 \cdot 10^{10}$ cm^{-2}. The dislocations themselves usually have many kinks, as shown in Figure 7A and 7B, indicating that the dislocations are pinned at many points presumably by impurities and imperfections in the lattice. A particularly interesting configuration of lattice defects is shown in Figure 7B; in this instance, besides heavily kinked dislocations, a great number of small dislocation loops are seen, usually elongated, with a length ranging from 200 to 1000Å. These loops are arranged in long rows which are closely parallel to certain crystallographic directions and sometimes extend entirely across a crystal fragment as shown in Figure 7B. Such rows of dislocation loops are presumably caused by the disintegration of elongated dislocation dipoles, first created by the anchoring of a dislocation at a single point followed by propagation in a direction parallel to the long axis of the dipole. The black particles in Figure 7B are fragments of ballas adhering to the surface of the specimen; true inclusions, as ascertained by the geometry of dislocations in their vicinity, were only rarely observed.

The above observations indicate that plastic deformation in ballas is significantly inhibited by impurities within the diamond lattice. The fact that ballas has been reported to be a relatively good electrical conductor (Sutton, 1928), presumably due to doping of the diamond lattice, further substantiates this point. Furthermore, Malov (1969) has observed inhibition of dislocation motion in synthetic

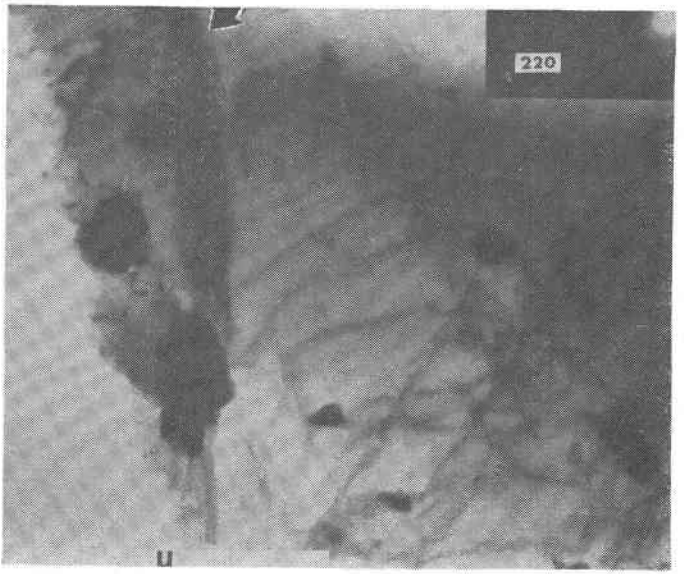

FIG. 6. Transmission electron micrograph of ballas fragment, showing dislocations and low-angle grain boundary (arrow). Insert: Section of corresponding selected area diffraction diagram with 220 reflections from material on both sides of the grain boundary.

ballas, caused by the presence of stacking faults and microtwins as well as impurities.

The orientation of the crystallites in ballas was determined from transmission X-ray diffraction patterns using Mo$K\alpha$ radiation. They were recorded on a precession camera equipped with a tubular col-

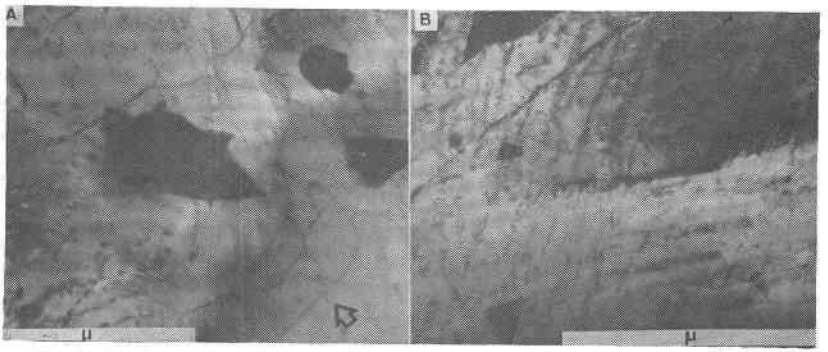

FIG. 7. Transmission electron micrographs of ballas. A: Kinked dislocations (near arrow). The black markings are fragments of diamond adhering to the thin film. B: An area containing many rows of dislocation loops.

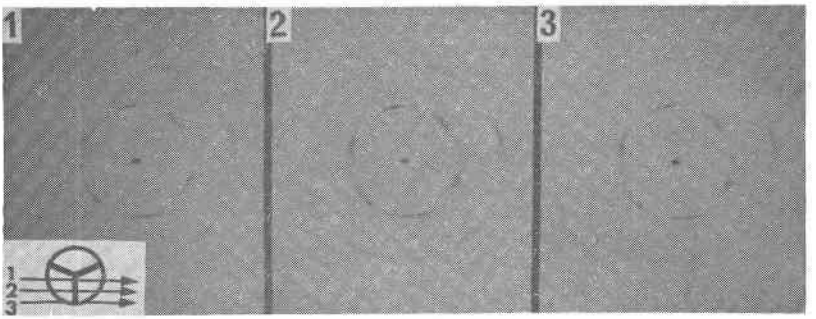

FIG. 8. X-ray patterns of ballas showing preferred orientation along [110]. The insert shows schematically the path of the rays with respect to the radial ridge on the fracture interface of the specimen for the three patterns.

limator with an exit diameter of 1.1 mm. Fractured specimens were mounted in such a way that the ridges radiating from their center were horizontal and at a right angle to the beam (see insert in Figure 8 where ridges are indicated by radial lines, and beam positions are indicated by the arrows). In this manner, several diffraction patterns could be obtained at a series of spots along an individual ridge, and several separate ridges could be investigated in the same specimen. Figure 8 shows three nearly identical diffraction patterns taken perpendicular to a single radial ridge, but at positions separated by approximately 1 mm. Preferred orientation of the fiber type with the [110] direction as the fiber axis is clearly evident, with a spread of about 15° about the mean position of the [110] fiber axis. Figure 9(2) shows a pattern taken from another ridge radiating from the center of the same specimen; after a slight rotation it is almost identical to the patterns shown in Figure 8.

When the ballas specimens were oriented in such a way that the beam of X-rays was parallel to radial ridges, ring patterns of the type shown in Fig. 9(1) were obtained invariably. This shows that the arrangement of diamond crystallites around the [110] texture axis is completely random.

For spherical ballas specimens, diffraction patterns taken anywhere on the surface using grazing incidence of the beam were similar to the ones given in Figure 8. Patterns taken through the center of the specimens were of the type shown in Figure 9(1). Similar results were obtained from the outer regions of an unusual specimen consisting of a clear single crystal of diamond 4 mm diameter at its center, surrounded by 1 mm thick, dark-gray polycrystalline layer.

Despite significant variations of the rocking angle of the arc-

shaped diffraction maxima ranging from ± 10 to ± 25°, the diffraction patterns taken perpendicularly to the ridges were similar in all instances to those given in Figure 8. This fully confirms the radial arrangement of crystallites in ballas.

As seen in Figures 8 and 9(2), the diffraction patterns exhibit the feature that one pair of arcs on the 111 ring is usually almost fused (at the arrow in Figure 9(1)), while the others are well separated. The same effects have been observed in explosively synthesized diamond (Trueb, 1971), which is also characterized by a [110] texture. This merely shows that the radial texture axis was tilted several degrees away from a position normal to the beam, as is confirmed by the strong 220 reflection on one side and its absence on the other.

Impurities and Inclusions

Examination of ballas specimens in the light microscope revealed several types of inclusions, both on the hemispherical outer surface and on fracture interfaces, as shown in Figure 10. Inclusions on outer surfaces of the stones were preferentially aggregated on grain boundaries; some examples can be seen in Figure 11A. Observation at high magnifications revealed that the spots outlining the grains were true inclusions so solidly anchored to the surrounding diamond matrix that they could not be extracted without pulverizing the entire ballas. In many instances it appeared that the bulk of such inclusions had been knocked out, leaving polyhedral pores which were fully or at least

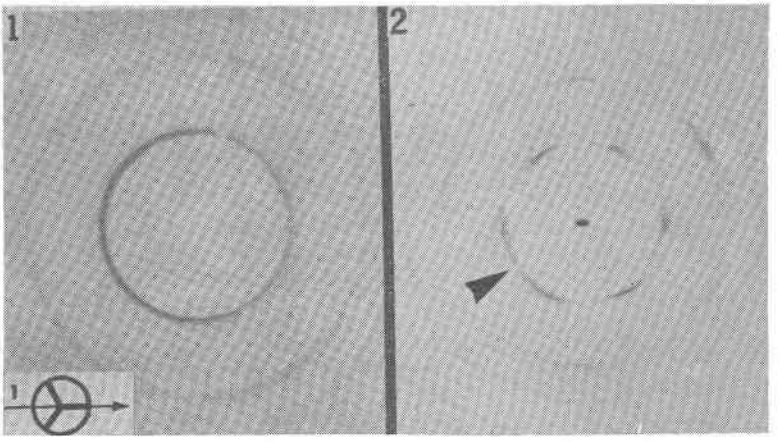

FIG. 9. X-ray patterns of ballas. 1: Ring diagram obtained with ray path along a ridge, as indicated in the insert. 2: Texture pattern obtained with ray path as given in Fig. 8. The arrow points to two fused 111 reflections.

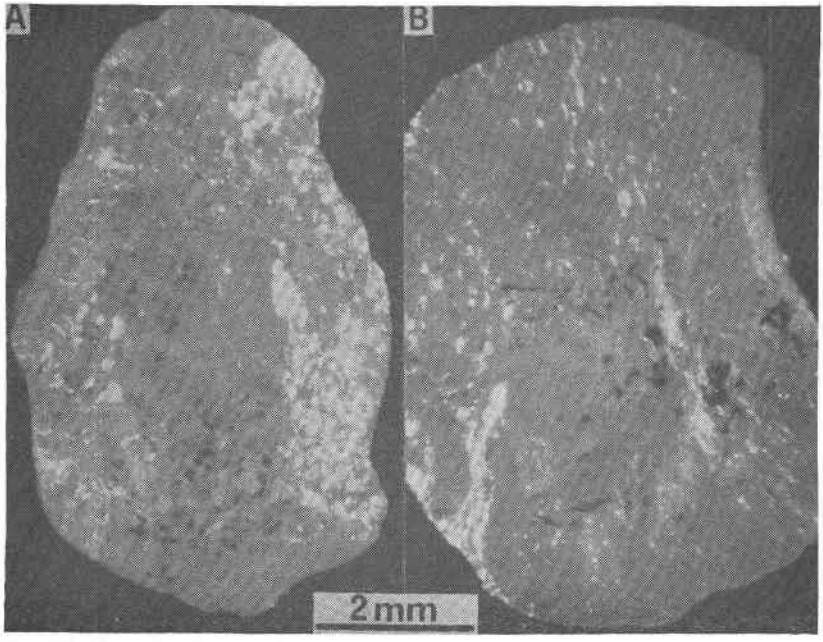

FIG. 10. Outer surface (A) and inner surface (B) of ballas showing various inclusions.

partly lined with black or dark-brown material. Inclusions on fresh fracture interfaces were usually clustered in certain areas of the ballas: thus the specimen shown in Figure 12B contained many inclusions throughout its center, but practically none at its periphery. Figure 11B shows part of a fracture interface rich in inclusions consisting of polyhedra with rounded edges.

Pure-white and pale-yellow ballas were transparent enough to allow observation, from the outside, of inclusions within the bulk of the stones, confirming the fact that the inclusions consisted of black particles and platelets sometimes clustered on grain boundaries, with a diameter occasionally exceeding 100 microns, but mainly in the 5 to 30 μm range.

A more detailed characterization of the shape and distribution of inclusions in ballas was undertaken by contact radiography with copper $K\alpha$ radiation on Kodak high-resolution plates. The radiographs were subsequently enlarged photographically. Approximately half of the radiographs were of the type shown in Figure 12A, characterized by isolated light spots indicating internal voids, and black spots indicating inclusions. The second type, of which Figure 12B is a

representative example, was characterized by a network of dark streaks apparently outlining grain boundaries and by isolated inclusions as well. Intermediate types with less dense networks of streaks were also quite common.

Ashing confirmed the results obtained by radiography. Fragments of ballas in a small platinum boat were burned in air at 1000°C. The clear stones yielded only a minute amount of pale–yellow ash in the form of loose fragments as shown in Figure 13A; in these the residue could not be weighed and the total impurity content was less than 0.2 percent. The combustion of dark ballas fragments yielded a coherent, pale–yellow skeletal structure retaining the shape of the original specimen; part of such a structure which resembles that seen in Figure 12B is shown in Figure 13B. Embedded in this skeleton were white crystallites with a diameter ranging from 5 to 30 microns, and porous black particles with a diameter up to 50 microns which appeared to have been partly melted or at least sintered to the skeletal structure during combustion of the ballas. Furthermore, white fluffy masses (Fig. 14A) and extended areas of very thin, transparent film showing interference colors and pierced by circular holes were also occasionally observed (Fig. 14A). A small area of this kind of film is also thought to have been observed by scanning electron microscopy on one of the very few fracture interfaces showing evidence of inter-

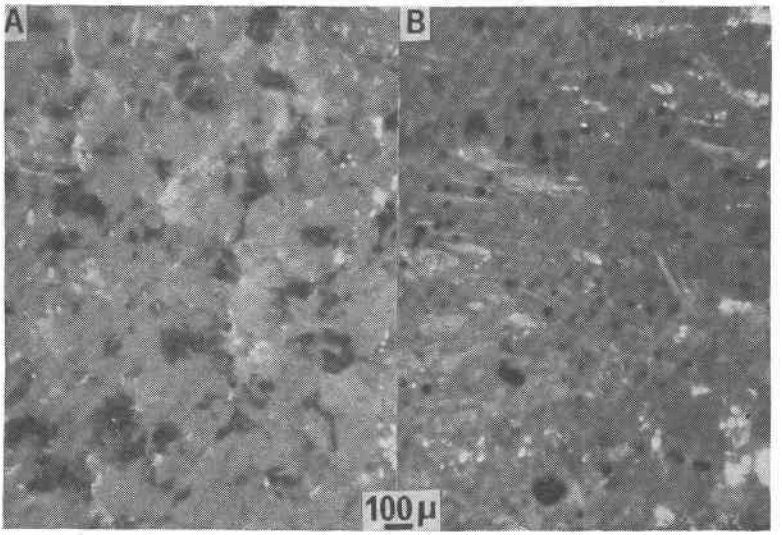

FIG. 11. Inclusions in ballas. A: An outer hemispherical surface. B: On fracture interface.

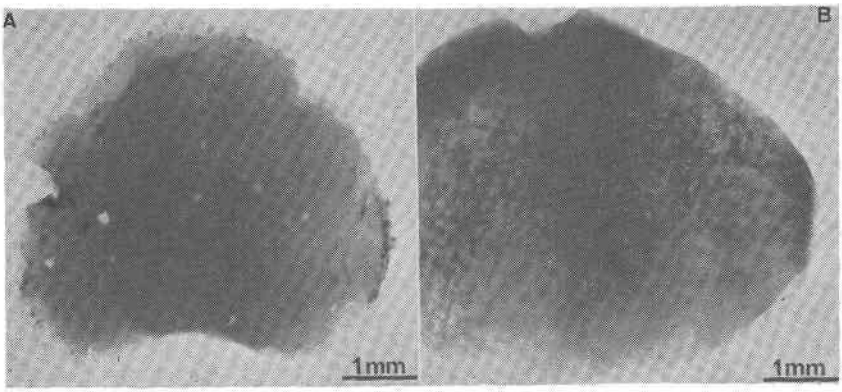

FIG. 12. Contact X-ray radiographs. A: Nearly pure-white ballas with very few inclusions. B: Dark-gray ballas with network of inclusions outlining grain boundaries.

granular failure (Fig. 14B). The highest level of impurities was 0.4 percent.

In order to determine the impurities in the bulk of ballas, the finely powdered fraction obtained by crushing the stones was analyzed by emission spectroscopy. Only five elements were detected, at the following levels: magnesium 2–50 ppm, aluminum 100–150 ppm, silicon

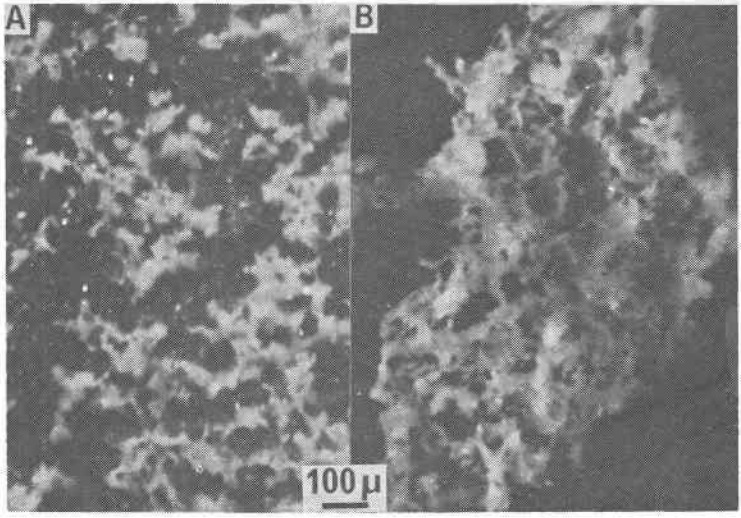

FIG. 13. Residue after combustion. A: Loose residue after combustion of clear ballas fragment. B: Skeletal structure left after combustion of dark-gray ballas fragment. (Compare with Fig. 12B).

200–500 ppm, titanium 20–200 ppm, iron 50–100 ppm. The concentration of forty-seven other common elements including the lanthanides was below the detectability limits of the instrument.

Electron probe microanalysis was used for *in-situ*, non-destructive characterization of inclusions. After vacuum-coating with carbon, element scans were made on visible inclusions protruding on fracture interfaces. It is worth noting that areas free of impurities and inclusions emitted an intense, violet-blue fluorescence when bombarded with 30 kV electrons, while stained areas where low levels of silicon and various metallic impurities were detected had a reddish-orange fluorescence. Most of the visible inclusions did not fluoresce. The predominant element in the inclusions was silicon, sometimes alone, but usually associated with iron, potassium and magnesium, or aluminum and calcium, or aluminum and iron. Small amounts of magnesium, titanium, and iron were found in almost all scans. Other elements observed occasionally in trace amounts were sulfur, chromium, manganese, nickel, zirconium, barium, lanthanum, cerium, neodymium, dysprosium, erbium, hafnium, and molybdenum. Some black inclusions gave only strong lines for iron with no detectable

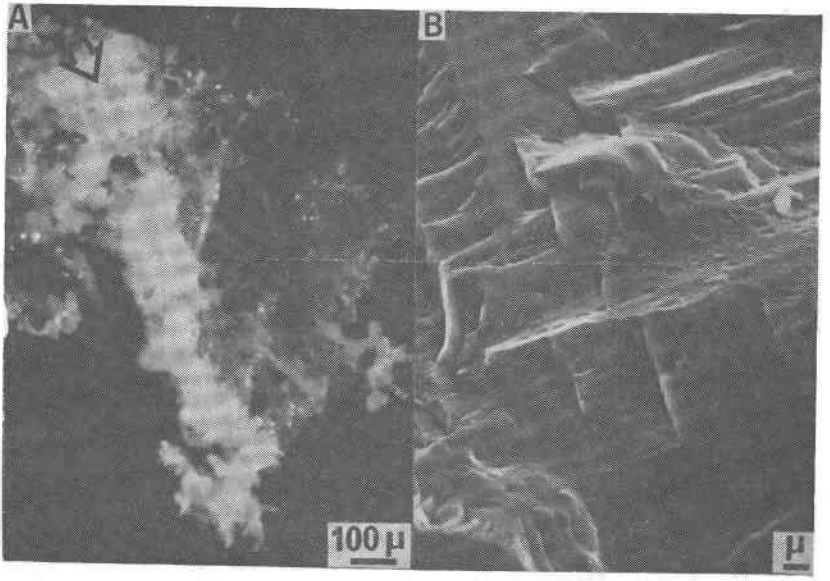

FIG. 14. A: Combustion residue of ballas fragment showing white fluffy material (arrow) and film-like structure (right). B: Scanning electron micrograph showing suspected film-like structure as in A causing intergranular fracture (arrow).

silicon, but with variable amounts of chromium and traces of other elements as listed above. Grain boundaries usually contained magnesium, aluminum, and silicon, occasionally associated with potassium, calcium, and various trace elements, particularly lanthanides.

Based on the association of elements detected on micron–size areas and the relative intensity of their fluorescent X–ray spectra, coupled with light–microscope observations, the following minerals are probably the principal inclusions in ballas: quartz, biotite, garnets (almandite and grossularite), diopside, hematite, chromite, gehlenite, phlogopite, and possibly pyroxene. Small amounts of ilmenite, zircon, and pyrite may also occur in association with the previously listed minerals. Most of the above are common inclusions in monocrystalline diamond, as cited by Williams (1932) and Lewis (1897), and are also commonly found in kimberlite.

The residue left after combustion of ballas fragments was also subjected to electron probe microanalysis; in a number of instances X–ray powder patterns of the same particles were also recorded. This allowed the unambiguous identification or confirmation of a number of minerals, although one must be aware that combustion at 1000°C and possibly higher localized temperatures due to the heat of combustion of the diamond matrix may have altered the chemical constitution of the inclusions and the original distribution of elements by interdiffusion and reaction between adjacent minerals. At any rate, the pale–yellow skeleton, the main residue left after combustion, was found to consist principally of andradite, grossularite, biotite, and augite with possible admixtures of quartz, ilmenite, rutile, and tourmaline. The black particles consisted of mixtures of hematite and magnetite, of chromite and possibly a calcium–iron oxide ($CaFe_2O_4$). The white crystallites isolated from the skeletal structures were identified as quartz, zircon, and grossularite. The fluffy white material shown in Figure 14A consisted almost entirely of quartz with admixtures of biotite and grossularite. The thin film–like structure also shown in Figure 14 was identified as corundum with small amounts of spinels (hercynite and pleonaste). In addition to the trace elements already listed, small amounts of bismuth and uranium were detected in various fractions of the ash.

It is worth noticing that our investigations confirm the occurrence of zircon as an inclusion in ballas; its occurrence in monocrystalline diamond was suspected by Williams (1932). Furthermore, quartz, which has never been found in African diamond but has been reported in Brazilian diamond by Bauer and Spencer (cited by Williams, 1932), is relatively plentiful in ballas.

Summary and Conclusions

From the results presented in the previous section, it can be concluded that ballas consists of anhedral, 30–40 micron crystallites of diamond indented into each other and possessing a texture radiating from a common center with a [110] fiber axis along each radius. Inclusions of various silicate minerals and metal oxides are found within the crystallites and in highly variable amounts along grain boundaries. Dislocation motion is significantly affected within the lattice by pinning; the latter effect as well as the interlocking of the grains, the almost complete lack of porosity, and possibly also the preferred orientation of the crystallites, appear to be mainly responsible for the unique physical properties of ballas.

Ballas thus appears to be a form of diamond intermediate between monocrystalline diamond on the one hand which contains few impurities in the lattice and is the result of slow growth under stable pressure–temperature conditions, and carbonado on the other hand which consists of random, porous aggregates of crystallites occluding considerable amounts of impurities and is presumed to be formed during a rapid change of pressure–temperature conditions. In the case of ballas, the radial growth pattern of the crystallites, their preferred orientation and their relatively narrow size distribution leaves little doubt that the growth of ballas proceeds from a central nucleus under conditions favoring nucleation and oriented growth. However, the mechanism that provides periodic stopping of crystal growth at a certain size, which results in three–dimensional bunching of linear aggregates consisting of similarly oriented crystallites, is not presently understood. Overall, the structure of ballas is somewhat reminiscent of spherulites, although the two main characteristics of spherulites, *i.e.*, needle–shaped crystals and non–crystallographic branching, have not been observed in ballas. A growth mechanism controlled by an impurity–rich boundary layer as cited by Keith and Padden (1963) to explain cellular growth may possibly apply for ballas.

Nikol'skaya *et al.* (1968) have recently characterized ballas as spherulites, with segmented radial rays in which the [111] direction is radial. This conclusion, which is at variance with our finding of a [110] texture, appears not to be supported by the X–ray patterns published by the above authors. If their patterns, as well as those described by Fischer (1961) were made by insufficiently collimated beams, the true texture might have been hidden by the overlapping of reflections from divergent fiber axes, a situation carefully avoided in our own work.

Acknowledgments

This work was supported by National Science Foundation grant GK 29571. The assistance of B. W. Dunnington (Glennel Corp., West Chester, Pennsylvania) in procuring the specimens and searching the literature on ballas is gratefully acknowledged. We also wish to thank T. Yamamoto (JEOLCO USA, Inc., Medford, Massachusetts) and M. D. Coutts (RCA Laboratories, Princeton, New Jersey) for the scanning electron micrographs.

References

Barrett, C. S. (1945) A new microscopy and its potentialities. *Trans. AIME,* **161,** 15–64.

Cumming, J. D. (1951) *Diamond Drill Handbook.* J. K. Smith and Sons of Canada, Ltd., Toronto.

Fischer, B. (1961) The 'ballas' form of diamond. *Nature,* **189,** 50.

Grodzinski, P. (1943) *Diamond and Gem Stone Industrial Production.* N.A.G. Press Ltd., London, 234.

Kalashnikov, Y. A., L. F. Vereshchagin, E. M. Feklichev, and I. S. Sukhushina (1967) Artificial production of a ballas-type diamond. *Dokl. Akad. Nauk SSSR,* **172,** 76 [transl. *Sov. Phys. Dokl.* **12,** 40 (1967)]

Keith, H. D., and F. J. Padden (1963) A phenomenological theory of spherulitic crystallization. *J. Appl. Phys.* **34,** 2409–2421.

Kunz, G. F. (1884) Five Brazilian diamonds. *Science,* **3,** 649–650.

Lewis, H. C. (1897) *Genesis and Matrix of the Diamond.* Longmans, Green and Co., London.

Malov, Y. V. (1969) Electron microscope study of artificial polycrystalline diamonds, ballas and carbonado. *Dokl. Akad. Nauk SSSR,* **186,** 807–808 [transl. *Sov. Phys. Dokl.* **14,** 545–546].

Mears, W. H., and R. J. Bowman (1966) *Industrial Diamond Ass. Amer., Proc. Tech. Sess. March 7, 1966, Boca Raton, Florida.*

Nikol'skaya, I. V., L. F. Vereshchagin, Y. L. Orlov, E. M. Feklichev, and Y. A. Kalashnikov (1968) Comparative study of natural and synthesized ballases. *Dokl. Akad. Nauk SSSR,* **182,** 77–79 [transl. *Sov. Phys. Dokl.* **13,** 881–883 (1969)].

Sutton, J. R. (1928) *Diamond.* Murby, London, **15,** 38.

Trueb, L. F. (1968) An electron-microscope study of shock-synthesized diamond. *J. Appl. Phys.* **39,** 4707–4716.

——— (1971) Microstructural study of diamonds synthesized under conditions of high temperature and moderate explosive shock pressure. *J. Appl. Phys.* **42,** 503–510.

———, and W. C. Butterman (1969) Carbonado: A microstructural study. *Amer. Mineral.* **54,** 412–425.

———, and E. C. De Wys (1969) Carbonado: Natural polycrystalline diamond. *Science,* **165,** 799–802.

———, and ——— (1971) Carbon from Ubangi—a microstructural study. *Amer. Mineral.* **56,** 1252–1268.

Wentdorf, R. N., and H. P. Bovenkerk (1961) On the origin of natural diamonds. *Astrophys. J.* **134,** 995–1005.

Williams, A. F. (1932) *The Genesis of Diamond.* Vol. 2. Benn, London. 470–480.

Manuscript received, March 14, 1972; accepted for publication, June 6, 1972.